CONFERENCE PRE-PRINT

DEUTERIUM GAS-DRIVEN PERMEATION AND RETENTION IN LA₂O₃, Y₂O₃, AND ZRO₂ DISPERSION-STRENGTHENED TUNGSTEN

Z.S. GAO, Z. CHEN, L. LI, Y.Y. LI, N. ZHANG, Z. LIU, C. YIN, S.F. MAO, M.Y. Ye University of Science and Technology of China Hefei, China

Email: zechen@ustc.edu.cn; yemy@ustc.edu.cn

Abstract

Oxide dispersion-strengthened tungsten (ODS-W) is a promising candidate for plasma-facing materials in future fusion reactors. However, the behavior of hydrogen isotopes in ODS-W has not yet been extensively investigated. In this study, the deuterium (D) permeation and retention behaviors of three ODS-W materials—W-La₂O₃ (WLaO), W-Y₂O₃ (WYO), and W-ZrO₂ (WZrO)—were systematically examined. The microstructures were characterized by backscattered electron (BSE) imaging and electron backscatter diffraction (EBSD), and distinct particle sizes and grain features among the three materials were analyzed. Besides, D₂ gas-driven permeation experiments were performed. Results indicate that WLaO and WYO exhibit similar permeabilities, but slightly lower than that of WZrO. Moreover, the D retention behavior is revealed by thermal desorption spectroscopy (TDS). The desorption peak of WLaO appears at a relatively high temperature at 1386.8 K, and WYO displays a double peak at 773.7 K and 1056.6 K. Meanwhile, WZrO exhibits a single peak at with a desorption flux more than one order of magnitude higher than the other two ODS-W. In addition, the retention behavior was further discussed in relation to the microstructural features.

1. INTRODUCTION

Tungsten (W) is the most promising candidate first wall material for fusion reactors due to its high melting point, high thermal conductivity, low sputtering yield, and low tritium retention [1-3]. However, W also faces several drawbacks, including high ductile-brittle transition temperature (DBTT), embrittlement under irradiation, and recrystallization [4-6]. The studies have shown that oxide-dispersion-strengthened W (ODS-W) with small amounts of oxide particle additions (e.g., La₂O₃, Y₂O₃, ZrO₂, Ce₂O₃) can not only effectively hinder dislocation slip and grain boundary migration in the W matrix, but also act as effective traps for irradiation defects [7-9]. Hence enhancing the high-temperature mechanical properties and toughness of W, reducing its DBTT, and improving its recrystallization temperature as well as irradiation resistance [10].

The permeation and retention of fusion fuel in first-wall materials are closely related to critical issues such as plasma steady-state operation, fuel cycle efficiency, and radiation safety [11]. However, hydrogen isotopes (HIs) behavior in ODS-W has not yet been systematically studied. Y. Sun *et al.* [12] investigated deuterium (D) retention in W-La₂O₃ materials under 40 eV D plasma irradiation and found that the D retention in W-La₂O₃ was about 30% higher than that in pure W. M. Zhao *et al.* [13] performed nuclear reaction analysis on W-Y₂O₃ and pure W after D plasma irradiation, and found that while local D concentrations differed, the total D retention was comparable. These studies have mainly focused on the surface blistering behavior of ODS-W under D plasma irradiation and the influence of irradiation parameters on D retention. Meanwhile, the investigations on D permeation behavior in ODS-W have been rarely reported.

In this study, the D permeation and retention behaviors in three types of ODS-W materials—W-La₂O₃, W-Y₂O₃, and W-ZrO₂—were systematically investigated to reveal their intrinsic responses to D. The permeabilities of these three ODS-W are measured and compared in the temperature range of 973-1123 K on a gas-driven permeation (GDP) device. Meanwhile, the D retention behaviors were examined through thermal desorption spectroscopy (TDS) experiments. In addition, the retention behavior was further discussed in relation to the microstructural characterization results.

2. EXPERIMENT

2.1. Materials and Sample preparation

The materials used in the experiments were ODS-W produced by AT&M Co. Ltd Inc., China, consisting of 2.0 wt% La₂O₃ (denoted as WLaO), 2.0 wt% Y₂O₃ (denoted as WYO), and 1.0 wt% ZrO₂ (denoted as WZrO). The

materials were processed into plates of 13 mm \times 70 mm \times 100 mm by hot rolling, and specimens were extracted perpendicular to the rolling direction using electrical discharge machining. Disk-shaped samples with a diameter of 12.6 mm and a thickness of 1 mm were prepared for GDP experiments, while square samples with dimensions of 10 mm \times 10 mm \times 1 mm were prepared for TDS experiments.

All samples were annealed at 1223 K for 2 h to remove residual gases. Subsequently, all samples were mechanically polished on both sides to achieve a mirror-like finish. For the square samples used in the TDS experiments, the four side surfaces were also mechanically polished to minimize the influence of surface morphology.

2.2. Gas-driven permeation and thermal desorption spectroscopy

The D permeation and retention experiments of ODS-W were carried out on the combined GDP and TDS platform at the University of Science and Technology of China. A detailed description of the experimental setup can be found in our previous work [14].

For the GDP experiments, the samples were placed between two silver-plated gaskets with an inner diameter of 6 mm and sealed in 1/4-inch VCR couplings (Swagelok Co., USA). A tubular furnace was used to provide the required experimental temperatures. After D_2 gas was introduced at a controlled upstream pressure, the permeated D signal downstream was monitored using a quadrupole mass spectrometer (PrismaPro® QMG 250, Pfeiffer Vacuum GmbH, Germany; detection mass range: 1-100 u). Measurements were conducted at temperatures ranging from 973 to 1123 K in 50 K intervals. At each temperature, measurements were performed under 3 upstream driving pressures ranging from $\sim 5 \times 10^4$ Pa to $\sim 1 \times 10^5$ Pa. D permeability at each temperature was derived from the steady-state D permeation flux, with measurements at varying upstream pressures providing the experimental error bars.

For the TDS experiments, D was introduced via static D_2 gas charging. Specifically, the samples were exposed to a D_2 atmosphere at 1173 K and $\sim 1 \times 10^5$ Pa for 2 hours, followed by rapid cooling to room temperature to trap D within the material. Thermal desorption was then performed. The D-charged samples were heated from room temperature to 1453 K at a constant rate of 0.5 K/s under high vacuum ($\sim 3 \times 10^{-5}$ Pa). The actual sample temperature was measured using an in-situ K-type armored thermocouple attached directly to the sample. The desorbed D signal was monitored by the quadrupole mass spectrometer. Analysis of the resulting TDS spectrum provided information on material defects and D retention.

3. RESULTS AND DISCUSSION

3.1. Microstructure characterization

The microstructure is a critical factor governing HIs permeation and retention in materials. For the three ODS-W materials investigated, scanning electron microscopy (SEM) was employed to perform backscattered electron (BSE) imaging, as shown in Fig. 1. Fig. 1(a-c) show the BSE images of WLaO, WYO, and WZrO, respectively. A clear contrast is observed between the dispersed oxide particles and the W matrix, indicating well-defined interfaces. The particle sizes of the three dispersoids differ significantly. Based on lower-magnification BSE images analyzed with ImageJ software [15], the size distributions of the dispersed particles were obtained in terms of equivalent circle diameter, as shown in Fig. 1(d-f). WYO has the largest average particle size, followed by WLaO, and WZrO has the smallest. In addition, a small fraction of coarse particles with diameters up to 10 µm is present in WYO. Moreover, the particle-W matrix interface densities of these materials were also quantified, and the results are listed in the third column of Table 1. It can be seen that WZrO, which has the smallest particle size, exhibits the highest particle-W interface density, which may influence D retention behavior in the material.

TABLE 1. GB density and W-particle interface density of ODS-W

Materials	LAGBs	HAGBs	W-particle interface
	$(\times 10^6 \text{ m}^{-1})$	$(\times 10^6 \text{ m}^{-1})$	$(\times 10^6 \text{m}^{-1})$
WLaO	0.53	0.18	0.15
WYO	1.32	1.08	0.11
WZrO	1.29	1.07	0.17

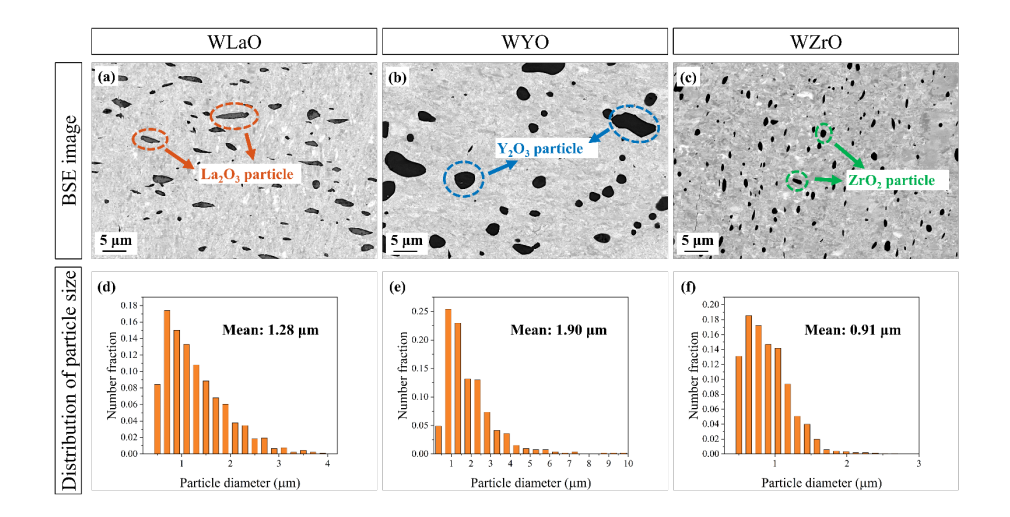


Fig. 1. BSE images of (a) WLaO, (b) WYO, and (c) WZrO, with dispersed oxide particles indicated by dashed circles. (d-f) Corresponding particle size distributions analyzed using ImageJ, with average sizes labeled in the plots. Each column corresponds to the same material.

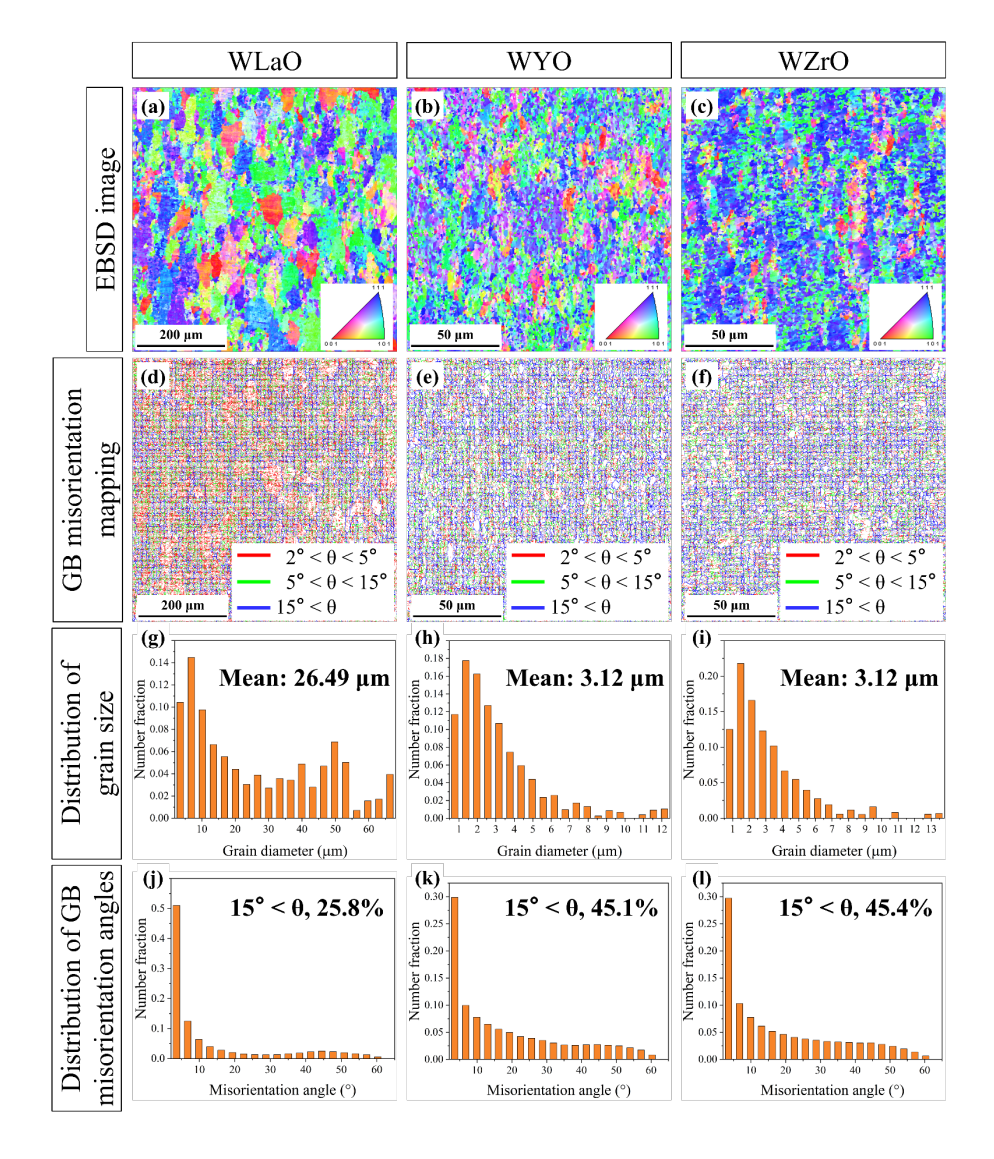


Fig. 2. EBSD results of (a) WLaO, (b) WYO, (c) WZrO with inverse pole figure maps. (d-f) GB maps with misorientation showing LAGBs and HAGBs. (g-i) Grain size distributions. (j-l) GB misorientation angle distributions. Each column corresponds to the same material.

Electron backscatter diffraction (EBSD) was employed to further characterize the grain structures of the three ODS-W materials, as shown in Fig. 2. For each material, the rows from top to bottom correspond to the grain orientation map, grain boundary distribution, grain size distribution, and misorientation angle distribution. From the grain orientation maps with inverse pole figures shown in Fig. 2(a-c), it can be observed that all three ODS-W materials exhibit multi-orientation distributions without the formation of a pronounced texture. Among them, the WLaO sample displays markedly coarser grains, whereas WYO and WZrO exhibit refined and relatively uniform grains. This suggests that Y2O3 and ZrO2 dispersoids play a more significant role in suppressing grain growth. The grain size distributions (Fig. 2(g-i)) further confirm these differences. WLaO shows an average grain size of ~26.49 μm with a broad distribution, and some grains exceeding 50 μm, indicating abnormal grain growth. In contrast, both WYO and WZrO exhibit average grain sizes of ~3.12 μm with relatively narrow distributions, among which WYO demonstrates better uniformity. The GB distributions (Fig. 2(d-f)) reveal the presence of GBs with various misorientation angles in all three materials. The corresponding misorientation angle distributions are shown in Fig. 2(j-1), while the statistical results of low-angle GBs (LAGBs, <15°) and high-angle GBs (HAGBs, >15°) are summarized in Table 1. It is evident that WLaO exhibits a relatively low GB density, dominated by LAGBs, with nearly half of these concentrated in the very low-angle range of 2-5°, indicating a prominent sub-grain characteristic. In contrast, both WYO and WZrO show a significantly higher GB density, with HAGBs accounting for more than 45% of the total. This demonstrates that a fine-grained structure has been effectively formed and that the dispersed particles exert a strong pinning effect [16] on GB migration.

3.2. Deuterium permeation behavior

Taking WYO as an example, the D permeation flux at different temperatures is shown in **Fig. 3(a)**. For each temperature, the three plateaus correspond sequentially to the increasing upstream driving pressures ($\sim 5 \times 10^4$ Pa, $\sim 7.5 \times 10^4$ Pa, and $\sim 1 \times 10^5$ Pa). In addition, **Fig. 3(b)** presents a good linear relationship between the steady-state permeation flux and the square root of the upstream pressure, indicating that the D driven permeation process through the material is dominated by bulk diffusion, with negligible influence from surface effects [17, 18]. Thus, the steady-state permeation flux can be expressed as:

$$J_{\infty} = \frac{\Phi}{I} p^{1/2} \tag{1}$$

where J_{∞} is the steady-state permeation flux, Φ is the permeability, L is the sample thickness, and p is the upstream driven pressure. Therefore, once the steady-state permeation flux is obtained, the permeability can be determined.

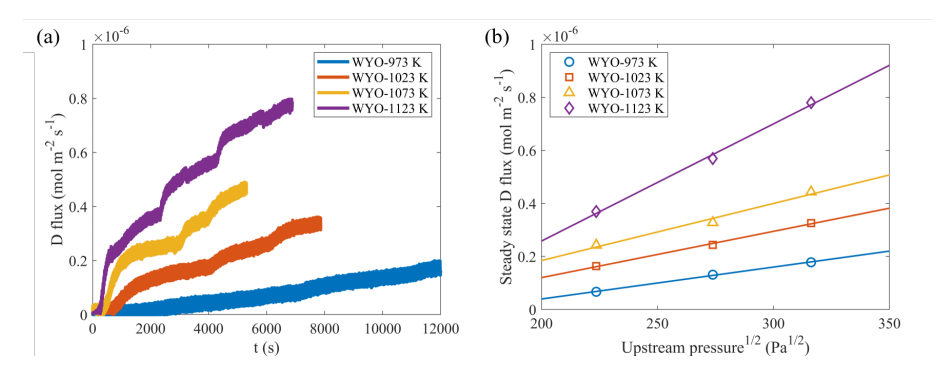


Fig. 3. D permeation results of WYO. (a) Permeation flux at different temperatures and upstream pressures of $\sim 5 \times 10^4$ Pa, $\sim 7.5 \times 10^4$ Pa, and $\sim 1 \times 10^5$ Pa. (b) Steady-state permeation flux as a function of the square root of upstream pressure at various temperatures.

The permeabilities of the three ODS-W materials measured in this work, together with those reported in the literature [14, 19, 20], are summarized in **Fig. 4**. As shown, the permeabilities of WLaO and WYO are very close to each other and slightly lower than that of WZrO. Overall, the permeabilities of the three ODS-W materials, as well as those of pure W and W-ZrC reported in the literature, are comparable, all falling within approximately the same order of magnitude. Such a similarity in permeability is understandable. Although the microstructures and internal defects of the materials differ, under steady-state permeation conditions hydrogen transport is predominantly governed by lattice diffusion [21], and the influence of microstructural variations becomes rather limited.

By fitting the experimental data in Fig. 4, the Arrhenius expressions for the permeability of WLaO and WYO are obtained as follows:

$$\Phi_{\text{WLaO}} = \left(1.84 \pm 4.82\right) \times 10^{-9} \exp\left(-\frac{0.68 \pm 0.24}{kT}\right), \text{ mol m}^{-1} \text{s}^{-1} \text{Pa}^{-1/2}, 1023 \text{ K} < T < 1123$$
 (2)

$$\Phi_{\text{WYO}} = \left(2.62 \pm 2.17\right) \times 10^{-8} \exp\left(-\frac{0.93 \pm 0.07}{kT}\right), \text{ mol m}^{-1} \text{s}^{-1} \text{Pa}^{-1/2}, 973 \text{ K} < T < 1123$$
 (3)

It should be noted that the permeability expression of WZrO is not given here, because in the experiment the D permeation signal of WZrO was only detected at two high-temperature points, which is insufficient for fitting. The obtained permeability constants for WLaO and WYO are 1.84×10^{-9} and 2.62×10^{-8} mol m⁻¹s⁻¹Pa^{-1/2}, respectively, with activation energies of 0.68 and 0.93 eV. Both values are slightly lower than the reported ranges for pure W [14, 19, 20], i.e., permeability constants of 3.20×10^{-8} and 3.21×10^{-7} mol m⁻¹s⁻¹Pa^{-1/2} and activation energies of 0.81-1.2 eV. This discrepancy may arise from two factors. The first one is the influence of GB density. Manhard *et al.* [22] studied hydrogen permeation in W by electrochemical methods and reported a low activation energy of only 0.39 eV, which they attributed to the high density of GBs in magnetron-sputtered W, where HIs may diffuse rapidly along the boundaries. The ODS-W materials in this study similarly exhibit a much higher GB density than pure W. The second factor is the effect of dispersed oxide particles. Buchenauer *et al.* [23] reported that, in low-temperature permeation experiments, oxygen released from metal oxides at elevated temperatures could oxidize the permeation membrane and influence the permeation process. Importantly, in their GDP experiments, these oxide impurities did not significantly influence the measured permeability. Although the dispersed oxide particles may partly explain the deviations in the permeability constants and activation energy relative to pure W, these factors do not substantially affect the overall permeability.

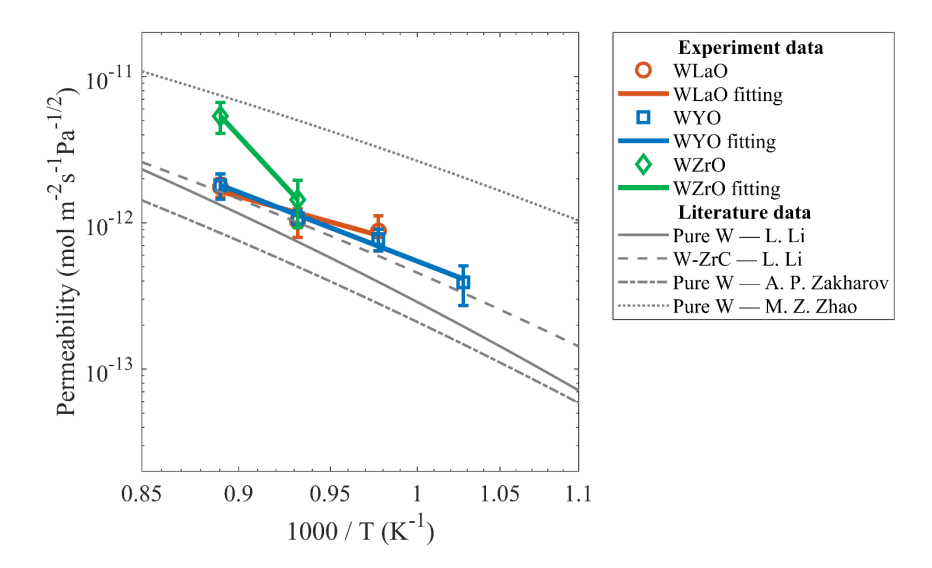


Fig. 4. The D permeability of WLaO, WYO, and WZrO compares with the references [14, 19, 20].

3.3. Deuterium retention behavior

The TDS spectrum of the three ODS-W, together with the previously obtained spectra of pure W [14], are summarized in Fig. 5. The background signal of D₂ can be neglected. It can be seen that the desorption peak of WLaO appears at a relatively high temperature, and the D signal is still not completely released even at a temperature close to 1500 K. The TDS spectrum of WYO exhibits a double peak, while WZrO shows a single peak but with a peak desorption flux more than one order of magnitude higher than that of the other materials. The analysis of the TDS spectra was carried out using a simplified MHIMS model [24], which only considers the desorption process during heating. Since gas charging was employed in this study, no additional defects were introduced during the process, and as the samples were rapidly cooled to room temperature and TDS were initiated within one hour after D₂ charging, it can be assumed that there was almost no mobile D. Thus, the D signals observed during TDS entirely originate from defects. The D concentration trapped in defects can be expressed as:

$$\frac{\partial C_{t,i}}{\partial t} = -v_0 C_{t,i} e^{-\frac{E_{T,i}}{kT}} \tag{4}$$

where $C_{t,i}$ is the concentration of trapped particles in the *i*th trap type, v_0 is the pre-exponential factor (or attempt frequency) in s⁻¹, and $E_{T,i}$ is the detrapping energy of the *i*th trap type. The detrapping energy and attempt

frequency were taken as fitting parameters, and the experimental desorption flux data were fitted using a least-squares method based on this equation. The detrapping energies corresponding to the experimental desorption peaks are summarized in **Table 2**. It is worth noting that the average attempt frequency obtained from the fitting is consistent in order of magnitude with that reported in the literature [14] using the Kissinger method with different heating rates.

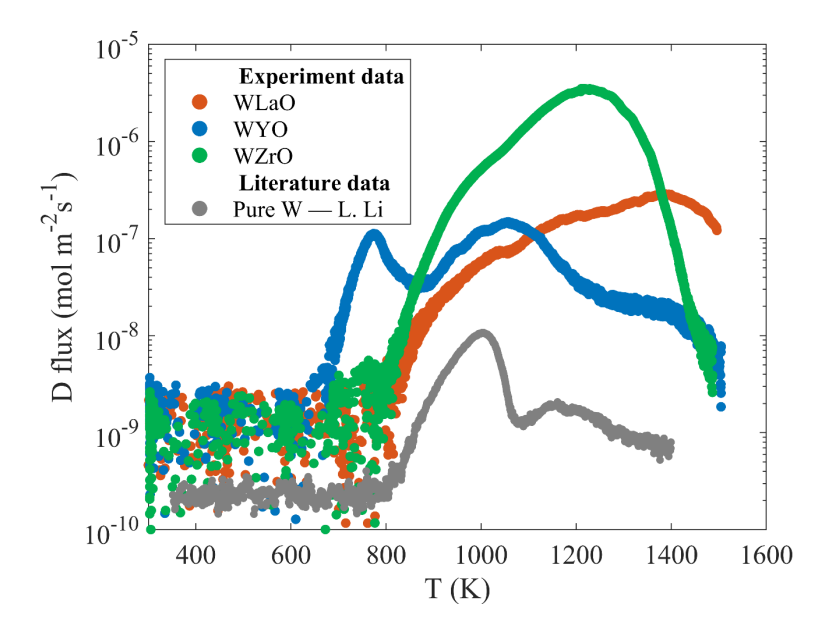


Fig.5. The TDS spectra of WLaO, WYO, and WZrO compares with the references [14].

TABLE 2. Desorption peaks in the TDS spectrum and corresponding detrapping energies

Materials	Peak (K)	$E_{T,i}$ (eV)
WLaO	1386.8	1.34
WYO	773.7; 1056.6	0.73; 1.02
WZrO	1228.4	1.19

Regarding the correlation between detrapping energy and material defects, Persianova *et al.* [25] reviewed extensive data on hydrogen desorption energies in W and reported 83 values associated with six types of traps. The detrapping energy for dislocation defects range from 0.65 to 1.25 eV, while those for the first hydrogen atom trapped at vacancies fall within 1.05 to 1.55 eV. These values do not adequately explain the present results, since ODS-W materials, in addition to GBs, also contain a large number of interfaces between oxide particles and the W matrix as well as the particles themselves, which serve as additional trapping sites. In WYO, the desorption peak at 1056.6 K and the corresponding desorption energy of 1.02 eV are close to those associated with GBs in pure W, which may suggest that this trap type is related to GB. However, no desorption peak near 1000 K was detected in the other two materials. This indicates that the GB contribution was masked by other defects (such as particles and particle-W matrix interfaces), making further analysis difficult. At present, the database of desorption energies associated with these extra defects remains highly limited.

Based on the microstructural characterization in this study, the contribution of different defects to the overall D retention is preliminarily discussed. The GB densities and particle-W matrix interface densities of the three ODS-W materials and pure W are summarized in **Table 1**. These results are plotted as stacked bar charts in **Fig. 6**. In addition, the total D retention of these materials, calculated by integrating the TDS spectra over time, is also shown in **Fig. 6**, marked with red dots and connected by dashed lines. The total D retention and GB densities in pure W is taken from the literature [14]. It can therefore be assumed that the trapping capacity of GBs in ODS-W is comparable to that in pure W. For WLaO, both the LAGBs and HAGBs densities are similar to those of pure W. However, its D retention is nearly two orders of magnitude higher, indicating that the majority of retention originates from particle-W matrix interfaces and the particles themselves. In the cases of WYO and WZrO, the GB densities are intrinsically much higher than in pure W. Nevertheless, despite having comparable grain boundary and interface densities, the D retention of WYO and WZrO differs by more than one order of magnitude.

This difference is most likely attributable to differences in the trapping capacity of Y_2O_3 and ZrO_2 particles. Unfortunately, a quantitative assessment of the contributions of individual defects to D retention in ODS-W materials cannot be provided in this study. Although some studies have suggested that hydrogen trapped at interfaces in WYO is more difficult to desorb than hydrogen in the W matrix [26], no quantitative relationship has been established. Moreover, for WLaO and WZrO, no reports are currently available regarding the trapping capacity of their particles or particle-W matrix interfaces. Future studies will require more computational work to assess the hydrogen-trapping capabilities of interfaces and the particles.

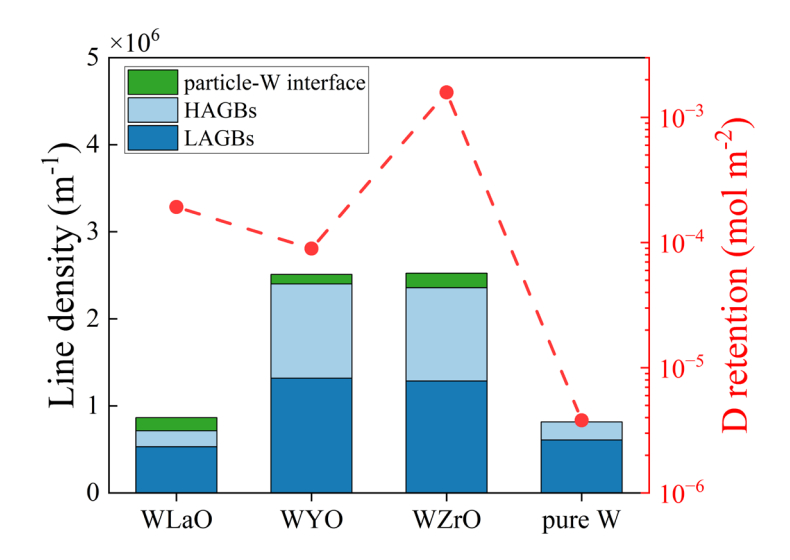


Fig. 6. Defect densities and D retention in pure W and ODS-W materials. Individual contributions from gGBs (LAGB and HAGB) and particle-W matrix interfaces are shown as stacked bars, while total D retention is indicated by red dots.

4. CONCLUSIONS

In this study, the D permeation and retention behaviors of three ODS-W materials were systematically investigated. Microstructural characterization by BSE and EBSD revealed distinct particle sizes and grain features. WYO exhibited the largest particles, WLaO was intermediate, and WZrO had the smallest particles. WYO and WZrO also showed refined and relatively uniform grains, whereas WLaO had coarser grains. GDP experiments indicated that WLaO and WYO have similar permeabilities, slightly lower than that of WZrO. Furthermore, TDS spectra showed that WLaO exhibits a high-temperature desorption peak, WYO displays a double peak, and WZrO presents a single peak with a desorption flux one order of magnitude higher than the others. These results reflect the combined influence of grain boundaries, particle-W matrix interfaces, and the dispersed particles. Overall, these findings provide a systematic understanding of D behavior in ODS-W materials, which is crucial for their application in fusion reactor first-wall components.

ACKNOWLEDGEMENTS

This work is supported by the National Natural Science Foundation of China (Grant No. U2267208), and the Fundamental Research Funds for the Central Universities (Grant no. WK2140000018).

REFERENCES

- [1] H. Bolt, V. Barabash, W. Krauss, J. Linke, R. Neu, S. Suzuki, N. Yoshida, A.U. Team, Materials for the plasma-facing components of fusion reactors, Journal of Nuclear Materials 329-333 (2004) 66-73.
- [2] R.A. Pitts, S. Carpentier, F. Escourbiac, T. Hirai, V. Komarov, S. Lisgo, A.S. Kukushkin, A. Loarte, M. Merola, A. Sashala Naik, R. Mitteau, M. Sugihara, B. Bazylev, P.C. Stangeby, A full tungsten divertor for ITER: Physics issues and design status, Journal of Nuclear Materials 438 (2013) S48-S56.
- [3] R.A. Pitts, X. Bonnin, F. Escourbiac, H. Frerichs, J.P. Gunn, T. Hirai, A.S. Kukushkin, E. Kaveeva, M.A. Miller, D. Moulton, V. Rozhansky, I. Senichenkov, E. Sytova, O. Schmitz, P.C. Stangeby, G. De Temmerman, I. Veselova, S. Wiesen, Physics basis for the first ITER tungsten divertor, Nuclear Materials and Energy 20 (2019).

- [4] J. Linke, J. Du, T. Loewenhoff, G. Pintsuk, B. Spilker, I. Steudel, M. Wirtz, Challenges for plasma-facing components in nuclear fusion, Matter and Radiation at Extremes 4(5) (2019).
- [5] S.J. Zinkle, L.L. Snead, Designing Radiation Resistance in Materials for Fusion Energy, Annual Review of Materials Research 44(1) (2014) 241-267.
- [6] S.J Zinkle, N.M Ghoniem, Operating temperature windows for fusion reactor structural materials, Fusion Engineering and Design 51–52 (2000) 55-71.
- [7] A. Sayir, Carbon fiber reinforced hafnium carbide composite, Journal of materials science 39(19) (2004) 5995-6003.
- [8] Y.-l. Wang, X. Xiong, G.-d. Li, H.-b. Zhang, Z.-k. Chen, W. Sun, X.-j. Zhao, Microstructure and ablation behavior of hafnium carbide coating for carbon/carbon composites, Surface and Coatings Technology 206(11-12) (2012) 2825-2832.
- [9] F. Xiao, Q. Miao, S. Wei, T. Barriere, G. Cheng, S. Zuo, L. Xu, Uniform nanosized oxide particles dispersion strengthened tungsten alloy fabricated involving hydrothermal method and hot isostatic pressing, Journal of Alloys and Compounds 824 (2020).
- [10] C. Luo, L. Xu, L. Zong, H. Shen, S. Wei, Research status of tungsten-based plasma-facing materials: A review, Fusion Engineering and Design 190 (2023).
- [11] J. Roth, E. Tsitrone, A. Loarte, T. Loarer, G. Counsell, R. Neu, V. Philipps, S. Brezinsek, M. Lehnen, P. Coad, C. Grisolia, K. Schmid, K. Krieger, A. Kallenbach, B. Lipschultz, R. Doerner, R. Causey, V. Alimov, W. Shu, O. Ogorodnikova, A. Kirschner, G. Federici, A. Kukushkin, Recent analysis of key plasma wall interactions issues for ITER, Journal of Nuclear Materials 390-391 (2009) 1-9.
- [12] Y. Sun, S. Wang, C. Li, W. Guo, Y. Yuan, H. Zhang, P. Wang, L. Cheng, G.-H. Lu, Dependence of deuterium retention and surface blistering on deuterium plasma exposure temperature and fluence in lanthanum oxide doped tungsten, Nuclear Materials and Energy 32 (2022).
- [13] M. Zhao, W. Jacob, A. Manhard, L. Gao, M. Balden, U. von Toussaint, Z. Zhou, Deuterium implantation into Y 2 O 3 doped and pure tungsten: Deuterium retention and blistering behavior, Journal of Nuclear Materials 487 (2017) 75-83.
- [14] L. Li, Z. Chen, Z. Gao, Y. Li, Z. Liu, W. Lin, C. Yin, S. Mao, X. Wang, M. Ye, Deuterium gas-driven permeation and retention in ZrC dispersion-strengthened W and pure W, Journal of Nuclear Materials 604 (2025).
- [15] J. Schindelin, I. Arganda-Carreras, E. Frise, V. Kaynig, M. Longair, T. Pietzsch, S. Preibisch, C. Rueden, S. Saalfeld, B. Schmid, J.-Y. Tinevez, D.J. White, V. Hartenstein, K. Eliceiri, P. Tomancak, A. Cardona, Fiji: an open-source platform for biological-image analysis, Nature Methods 9(7) (2012) 676-682.
- [16] R. Doherty, D. Hughes, F. Humphreys, J.J. Jonas, D.J. Jensen, M. Kassner, W. King, T. McNelley, H. McQueen, A. Rollett, Current issues in recrystallization: a review, Materials Science and Engineering: A 238(2) (1997) 219-274. [17] H.H. Johnson, Hydrogen in iron, Springer, 1988.
- [18] Z. Chen, X. Hu, M. Ye, B.D. Wirth, Deuterium transport and retention properties of representative fusion blanket structural materials, Journal of Nuclear Materials 549 (2021).
- [19] M. Zhao, M. Nakata, F. Sun, Y. Hatano, Y. Someya, K. Tobita, Y. Oya, Deuterium Permeation Behavior in Fe Ion Damaged Tungsten Studied by Gas-Driven Permeation Method, Fusion Science and Technology 76(3) (2020) 246-251. [20] A. Zakharov, V. Sharapov, E. Evko, Hydrogen permeability of polycrystalline and monocrystalline molybdenum and tungsten, Soviet materials science: a transl. of Fiziko-khimicheskaya mekhanika materialov/Academy of Sciences of the Ukrainian SSR 9(2) (1975) 149-153.
- [21] A. McNabb, P.K. Foster, A new analysis of diffusion of hydrogen in iron and ferritic steels, Transactions of the Metallurgical Society of AIME 227(3) (1963) 618-&.
- [22] A. Manhard, S. Kapser, L. Gao, Electrochemical study of hydrogen permeation through tungsten near room temperature, Journal of Nuclear Materials 463 (2015) 1057-1061.
- [23] D.A. Buchenauer, R.A. Karnesky, Z.Z. Fang, C. Ren, Y. Oya, T. Otsuka, Y. Yamauchi, J.A. Whaley, Gas-driven permeation of deuterium through tungsten and tungsten alloys, Fusion Engineering and Design 109-111 (2016) 104-108. [24] E. Hodille, X. Bonnin, R. Bisson, T. Angot, C. Becquart, J. Layet, C. Grisolia, Macroscopic rate equation modeling of trapping/detrapping of hydrogen isotopes in tungsten materials, Journal of Nuclear Materials 467 (2015) 424-431.
- [25] A.P. Persianova, A.V. Golubeva, Hydrogen Traps in Tungsten: A Review, Physics of Metals and Metallography 125(3) (2024) 278-306.
- [26] S. Wen, X. Zhang, H. Deng, M. Pan, Investigation of the W/Y2O3 heterogeneous interface properties and its effect on hydrogen behavior using first-principles calculations, Nuclear Fusion 62(8) (2022) 086015.